Finite size effects on the Poynting-Robertson effect: a fully general relativistic treatment

Jae Sok Oh[1]

Department of Physics and Astronomy, FPRD,
Seoul National University, Seoul 151-742, Korea

Hongsu Kim[2]

KVN,
Korea Astronomy and Space Science Institute, Daejeon 305-348, Korea

Hyung Mok Lee[3]

Department of Physics and Astronomy, FPRD,
Seoul National University, Seoul 151-742, Korea

ABSTRACT

Even since the first discovery of Poynting and Robertson, the radiation source has been treated as merely a point. Even in a very few studies where the size of the source has been taken into account, the treatment of the problem remained largely non-relativistic. In the present work, we address the issue of the finite size effects on the Poynting-Robertson effect in a fully relativistic manner for the first time. As a result, the emergence and the characteristic of the critical point/suspension orbit can be studied in a systematic and detailed manner.
PACS numbers: 04.20.-q, 97.60.Jd, 95.30.Gv

[1]E-mail: ojs@astro.snu.ac.kr
[2]E-mail: hongsu@Kasi.re.kr
[3]E-mail: hmlee@snu.ac.kr

1 Introduction

Effects of the radiation field on a test particle orbiting a radiation source has been studied since the discovery of Poynting-Robertson effect [1] and [2]. We begin with the summary of the present status of research in the literature along this line. First, Guess [3] studied the effects of finite size and found that radiation drag (Poynting-Robertson effect) gets enhanced compared to the case of point-like radiation source. In his work he confined his calculation to first order in v/c. Second, Carrol [4] found that the finite size effect of the radiation source renders the radiation drag force greater than its counterpart for a point-like source. His treatment, however, was limited to the context of special relativity. Third, Abramowicz, Ellis, and Lanza [5] constructed the general relativistic radiation stress-energy tensor describing the radiation field from the non-rotating radiation source with finite radius size for the first time and solved the equation of motion to discover the existence and the location of a critical point at which all segments of accretion flow are captured. As their concern was to describe jets and outflows, they limited the particle's motion to one-dimensional radial motion alone. Fourth, Miller and Lamb [6] and [7] considered and solved the azimuthal as well as radial component of the equation of motion. They, however, failed to notice the emergence of and study the nature of critical point as they considered the set-up in which the luminosity of the radiation source is well below the Eddington critical value. Interestingly enough, lastly, Bini, Jantzen, and Stella [8] studied general relativistic version of the Poynting-Robertson effect by considering and solving all 3-components (time, radial, and azimuthal) of the equation of motion. Their set-up, however, is not identical to that in our present work in that they employed the radiation stress-energy tensor describing the radiation field from a point source. They ignored the finite size of the radiation source.

In the present work, in order to address general relativistic version of finite size effects on the Poynting-Robertson effect in a rigorous and complete manner, we employed the radiation stress-energy tensor first constructed by Abramowicz, Ellis, and Lanza [5] to explore the detailed impact of the radiation forces on the test particle's trajectories.

In section 2 we describe the derivation of the equation of motion of the test particle in the Schwarzschild space-time background outside a non-rotating, isotropic radiating spherical star with finite size. In section 3, we present the results of the numerical integrations along with the our analytical results. Finally in section 4, we summarize and discuss our results.

2 Equations of motion

To derive the equations of motion that govern the orbital motion of the test particle in the radiation field from the spherical star emitting the radiation isotropically, we start with Schwarzschild spacetime,

$$ds^2 = g_{\mu\nu} dx^\mu dx^\nu$$

$$= \quad -(1-2M/r)dt^2 \; + \; (1-2M/r)^{-1}dr^2 \; + \; r^2(d\theta^2 \; + \; \sin^2\theta d\phi^2). \tag{1}$$

We work in the geometric units, where $G = 1 = c$ (G is the gravitational constant and c is the speed of light). The equations of motion is given by

$$a^\alpha = \frac{f^\alpha}{m} \tag{2}$$

where f^α denotes a non-gravitational force (for example, radiation force) exerted by the radiation (or luminosity) on the test particle, m is the rest mass of the test particle, and

$$a^\alpha = \frac{dU^\alpha}{d\tau} \; + \; \Gamma^\alpha_{\mu\nu}U^\mu U^\nu \tag{3}$$

is the acceleration, where U^α is the four-velocity of the particle, $\Gamma^\alpha_{\mu\nu} = \frac{1}{2}g^{\alpha\beta}(g_{\beta\mu,\nu} + g_{\beta\nu,\mu} - g_{\mu\nu,\beta})$ is the Affine connection, and comma (,) denotes partial derivatives.

If we assume that the cross-section σ of the test particle is independent of energy (frequency) and direction of the photon, the non-gravitational force f^α due to scattering of photon from the star is given by [9],

$$f^\alpha = \sigma F^\alpha, \tag{4}$$

where F^α shown below is the quantity transformed from the radiation energy flux $T^{\hat{i}\hat{0}}_{co}$ measured in the particle's rest frame (which is comoving with the particle) using the orthonormal tetrad $\tilde{e}^\alpha_{\hat{i}}$ associated with the particle's rest frame as follows,

$$\begin{aligned} F^\alpha &= \tilde{e}^\alpha_{\hat{i}} T^{\hat{i}\hat{0}}_{co} \\ &= -h^\alpha_\beta T^{\beta\sigma} U_\sigma, \end{aligned} \tag{5}$$

where $h^\alpha_\beta = \delta^\alpha_\beta + U^\alpha U_\beta$ is the projection tensor, and $T^{\beta\sigma}$ is the radiation stress-energy tensor in the lab frame.

According to [5], the components of the radiation stress tensor $T^{\hat{\alpha}\hat{\beta}}$ measured in LNRF (Locally Non-Rotating Frame; [10, 11]) can be written as,

$$T^{\hat{t}\hat{t}} = 2\pi I(r)(1-\cos\alpha) \tag{6}$$

$$T^{\hat{t}\hat{r}} = \pi I(r)\sin^2\alpha \tag{7}$$

$$T^{\hat{r}\hat{r}} = \frac{2}{3}\pi I(r)(1-\cos^3\alpha) \tag{8}$$

$$T^{\hat{\theta}\hat{\theta}} = \frac{\pi}{3} I(r)(\cos^3\alpha - 3\cos\alpha + 2) \tag{9}$$

$$T^{\hat{\phi}\hat{\phi}} = \frac{\pi}{3} I(r)(\cos^3\alpha - 3\cos\alpha + 2), \tag{10}$$

where α is an apparent viewing angle of the star seen by an observer (FIDO; fiducial observer) at rest in the LNRF and is given by $\sin\alpha = \left(\frac{R}{r}\right)\left(\frac{1-2M/r}{1-2M/R}\right)^{1/2}$ (see [5]) for the radius of the star

$R \geq 3M$, and $I(r)$ is the frequency-integrated specific intensity at the radial position r and can be expressed as (see Appendix A in the [7])

$$I(r) = \frac{(1-2M/R)}{(1-2M/r)^2}\frac{mM}{\pi\sigma R^2}\left(\frac{L^\infty}{L^\infty_{Edd}}\right), \tag{11}$$

where L^∞ is the luminosity at infinity and L^∞_{Edd} is the Eddington critical luminosity, which is given by $L^\infty_{Edd} = 4\pi mM/\sigma$.

By transforming $T^{\hat{\mu}\hat{\nu}}$ using the tetrad $e^\alpha_{\hat{\mu}}$ associated with the LNRF, we can obtain the components of the radiation stress tensor $T^{\alpha\beta}$,

$$T^{\alpha\beta} = e^\alpha_{\hat{\mu}} e^\beta_{\hat{\nu}} T^{\hat{\mu}\hat{\nu}}, \tag{12}$$

where the tetrad associated with LNRF in the Schwarzschild coordinates is given by,

$$\begin{aligned} e^{\hat{0}} &= (1-2M/r)^{1/2}dt, \\ e^{\hat{1}} &= (1-2M/r)^{-1/2}dr, \\ e^{\hat{2}} &= r d\theta, \\ e^{\hat{3}} &= r\sin\theta d\phi. \end{aligned} \tag{13}$$

Finally, the radiation stress-energy tensor describing the radiation field from the radiation source of finite size ($R \geq 3M$) can be rewritten as,

$$T^{tt} = \left(\frac{m}{\sigma}\right)\frac{2}{(1+\cos\alpha)}\left(\frac{M}{r^2}\right)\left(1-\frac{2M}{r}\right)^{-2}\left(\frac{L^\infty}{L^\infty_{Edd}}\right) \tag{14}$$

$$T^{tr} = \left(\frac{m}{\sigma}\right)\left(\frac{M}{r^2}\right)\left(1-\frac{2M}{r}\right)^{-1}\left(\frac{L^\infty}{L^\infty_{Edd}}\right) \tag{15}$$

$$T^{rr} = \left(\frac{m}{\sigma}\right)\frac{2(1+\cos\alpha+\cos^2\alpha)}{3(1+\cos\alpha)}\left(\frac{M}{r^2}\right)\left(\frac{L^\infty}{L^\infty_{Edd}}\right) \tag{16}$$

$$T^{\theta\theta} = \left(\frac{m}{\sigma}\right)\frac{(2-\cos\alpha-\cos^2\alpha)}{3(1+\cos\alpha)}\left(\frac{M}{r^4}\right)\left(1-\frac{2M}{r}\right)^{-1}\left(\frac{L^\infty}{L^\infty_{Edd}}\right) \tag{17}$$

$$T^{\phi\phi} = \left(\frac{m}{\sigma}\right)\frac{(2-\cos\alpha-\cos^2\alpha)}{3(1+\cos\alpha)}\left(\frac{M}{r^4\sin^2\theta}\right)\left(1-\frac{2M}{r}\right)^{-1}\left(\frac{L^\infty}{L^\infty_{Edd}}\right). \tag{18}$$

When a radiation source is point-like, the apparent viewing angle (α) measured by FIDO is equal to zero, thus $\cos\alpha = 1$. Inserting this $\cos\alpha = 1$ into above equations (14) through (18) gives the radiation stress-energy tensor for point-like radiation source, which is exactly identical to the radiation stress-energy tensor employed by Bini, Jantzen, and Stella [8].

When the radius (R) of the radiation source is smaller than the photon sphere ($3M$), i,e., $R \leq 3M$, the apparent viewing angle is given by,

$$\sin\alpha = 3\sqrt{3}\left(\frac{M}{r}\right)\left(1-\frac{2M}{r}\right)^{1/2}. \tag{19}$$

Therefore, the radiation stress-energy tensor describing the radiation field from the radiation source which has a radius smaller than the photon sphere have no dependence of the source's radius R. Thus, such radiation sources can be treated as a radiation source with $R = 3M$(the radius of the photon sphere).

We can restrict the orbital motion of the particle to the equatorial plane ($\theta = \frac{\pi}{2}, U_\theta = 0$), without loss of generality owing to the spherical symmetry of non-rotating spherical star, thus the equation of motion finally can be decomposed into each components as follows;

$$\begin{aligned}\frac{dU_t}{d\tau} &= \left(\frac{M}{r^2}\right)\left[1-2\left(1-\frac{2M}{r}\right)^{-1}U_t^2\right]\left(\frac{L^\infty}{L^\infty_{Edd}}\right)U_r \\ &- \frac{(8+2\cos\alpha+2\cos^2\alpha)}{3(1+\cos\alpha)}\left(\frac{M}{r^2}\right)\left(\frac{L^\infty}{L^\infty_{Edd}}\right)U_tU_r^2 \\ &- \frac{(8-\cos\alpha-\cos^2\alpha)}{3(1+\cos\alpha)}\left(\frac{M}{r^4}\right)\left(1-\frac{2M}{r}\right)^{-1}\left(\frac{L^\infty}{L^\infty_{Edd}}\right)U_tU_\phi^2\end{aligned} \tag{20}$$

$$\begin{aligned}\frac{dU_r}{d\tau} &= -\left(\frac{M}{r^2}\right)\left(1-\frac{2M}{r}\right)^{-1}-\left(\frac{2M}{r^2}\right)U_r^2+\left(\frac{1}{r^3}\right)\left(1-\frac{2M}{r}\right)^{-1}\left(1-\frac{3M}{r}\right)U_\phi^2 \\ &- \left(\frac{M}{r^2}\right)\left(1-\frac{2M}{r}\right)^{-2}\left[1+2\left(1-\frac{2M}{r}\right)U_r^2\right]\left(\frac{L^\infty}{L^\infty_{Edd}}\right)U_t \\ &- \frac{(8+2\cos\alpha+2\cos^2\alpha)}{3(1+\cos\alpha)}\left(\frac{M}{r^2}\right)\left(1-\frac{2M}{r}\right)^{-1}\left[1+\left(1-\frac{2M}{r}\right)U_r^2\right]\left(\frac{L^\infty}{L^\infty_{Edd}}\right)U_r \\ &- \frac{(8-\cos\alpha-\cos^2\alpha)}{3(1+\cos\alpha)}\left(\frac{M}{r^4}\right)\left(1-\frac{2M}{r}\right)^{-1}\left(\frac{L^\infty}{L^\infty_{Edd}}\right)U_rU_\phi^2\end{aligned} \tag{21}$$

$$\begin{aligned}\frac{dU_\phi}{d\tau} &= -\left(\frac{2M}{r^2}\right)\left(1-\frac{2M}{r}\right)^{-1}\left(\frac{L^\infty}{L^\infty_{Edd}}\right)U_tU_rU_\phi \\ &- \frac{(8-\cos\alpha-\cos^2\alpha)}{3(1+\cos\alpha)}\left(\frac{M}{r^2}\right)\left(1-\frac{2M}{r}\right)^{-2}\left(\frac{L^\infty}{L^\infty_{Edd}}\right)U_t^2U_\phi \\ &- \cos\alpha\left(\frac{M}{r^2}\right)\left(\frac{L^\infty}{L^\infty_{Edd}}\right)U_r^2U_\phi.\end{aligned} \tag{22}$$

We are ready to envisage the features of the solution to the equation of motion. First, equation (21), radial component of equation of motion, includes four lines: the three terms in the first line is not relevant to the radiation. as overall sign of the second line is positive definite, this line can be identified with the outward radiation pressure gradient and it should be noted that the second line has no dependence of the finite size of the radiation source. Both third line

and fourth line can be regarded as being responsible for the radial radiation drag force as their overall sign are negative definite. As the third line depends on the radial velocity component alone, if we take into account only radial motion, the radial radiation drag is attributable to the third line. As we can know from the finite size dependent part ($\frac{(8+2\cos\alpha+2\cos^2\alpha)}{3(1+\cos\alpha)}$) of the third line, the radial radiation drag at the surface of the radiation source ($\cos\alpha = 0$) gets 4/3 times larger than that of the point-like source ($\cos\alpha = 1$), which is identical with the results in the study of Guess [3] and Carrol [4]. However, their study failed to mention about the our fourth line radiation drag which depends on both the radial velocity and the azimuthal velocity. The radial radiation drag in the fourth line gets 8/3 time large compared to the point-like source. Second, equation (22), azimuthal component of equation of motion, is composed of three lines: the first line depends on both the radial and the azimuthal velocity and its overall sign relies on the direction of the radial motion of the particle. When the particle is in inward motion, as its overall sign is negative definite, the first line can be regarded as the azimuthal radiation drag, but if the motion of the particle is changed to outward one, as its overall sign is changed to positive definite, it can be identified with the radiation counter-drag. As the second line has a dependence of the azimuthal velocity only and its overall sign is negative definite, this second line can be regarded as the azimuthal radiation drag exerted on the particle in circular motion. The finite size dependent part in the second line indicates that the azimuthal radiation drag at the surface of the radiation source gets 8/3 times larger than that of the point-like source, which also is identical with the results in the study of Guess [3] and Carrol [4]. Finally, the third line depends on both the radial and the azimuthal velocity and its overall sign is negative definite, thus this third line can be also identified with the radiation drag. Interestingly, the finite size of the radiation source leads to smaller radiation drag than a point-like source.

3 Results of numerical integration

For the sake of convenience, we introduce luminosity parameter $L \equiv \frac{L^\infty}{L^\infty_{Edd}}$.

Figure 1 shows the ways the test particle arrives and enters onto the dotted circle. The test particle arriving at the dotted circle seems to be suspended and not to move any more there, thus hereinafter we will refer to the dotted circle as "suspension orbit". The starting points of the particle are the same as $(6M, 0)$ in Cartesian coordinates (X,Y). Initial azimuthal velocities are fixed to be 0.2c and its direction is counterclockwise. Also, the luminosity of the radiation sources are the same as $L = 0.8$. Radial distance of the "suspension orbit" is roughly $r_{so} \simeq 5.56M$. Solid line denotes the trajectory of the test particle when the radiation source is point-like, and dotted, dashed, and long dashed lines denote the trajectories of the particle when the radiation sources have the radii of 3M, 4M, and 5M, respectively. As it is mentioned above section II, it should be noted that the radiation source with radius smaller than $3M$ (photon sphere) can be treated as one with radius of $3M$.

As shown in Figure 1, as the size (radius) of the radiation source gets larger, the "suspension orbit" stays the same (location) but the test particle arrives at the "suspension orbit" more and

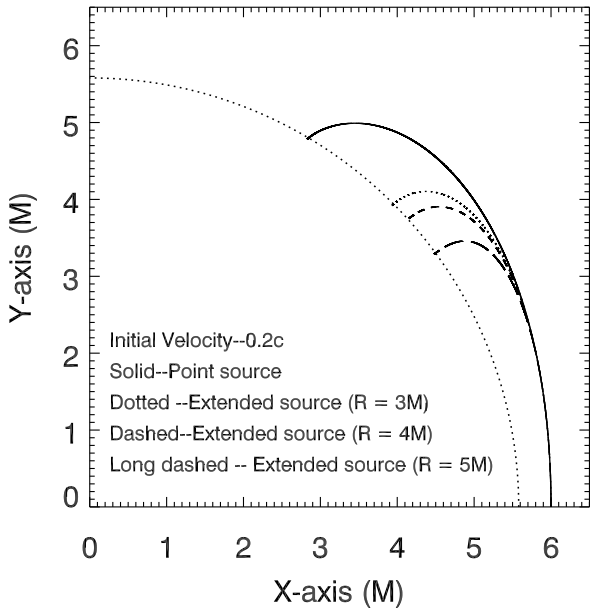

Figure 1: shows the ways the test particle arrives and enters onto the suspension orbit. 4-trajectories provided exhibit as the radiation source gets larger and hence it's surface gets wider, the Poynting-Robertson effect gets more and more manifest reducing the test particle's azimuthal speed more and more remarkably. The luminosity parameter of the radiation sources are the same as $L = 0.8$ and dotted circle denotes "suspension orbit".

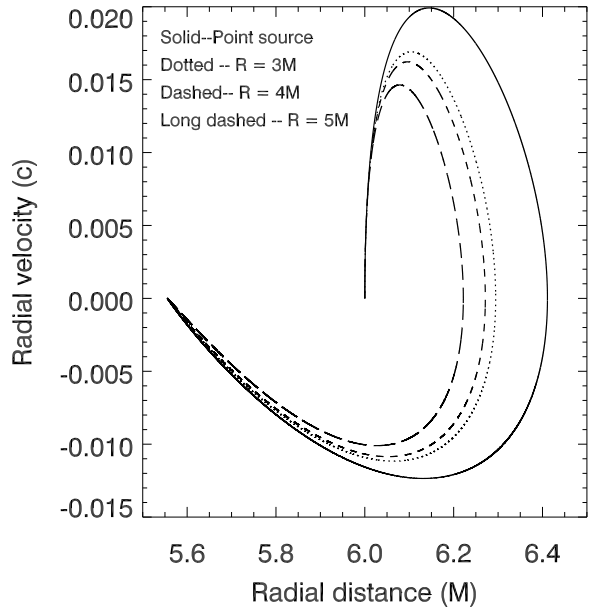

Figure 2: demonstrates the radial velocity profiles of the 4-trajectories of the test particle given in Figure 1.

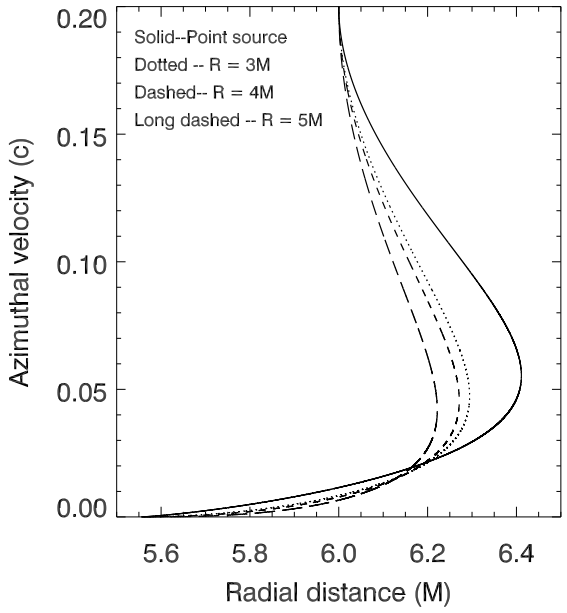

Figure 3: demonstrates the azimuthal velocity profiles of the 4-trajectories of the test particle given in Figure 1.

more quickly. Unlike the case of the point source where the test particle hits the "suspension orbit" at some finite angle, when the source has finite size, the test particle always strikes the "suspension orbit" nearly perpendicularly.

Figures 2 and 3 demonstrate the radial and azimuthal velocity profiles of the 4-trajectories of the test particle given in Figure 1, respectively. As shown in Figures 2 and 3, around the "suspension orbit", as the size of the radiation source gets larger, the radial and azimuthal velocities are more and more quickly reduced and finally vanish at the "suspension orbit". Thus, from Figures 1 through 3 we can find out that the radial and azimuthal velocities of the test particle at the "suspension orbit" are, respectively, equal to zero and the rate of change of the radial and azimuthal velocities also vanish, respectively, hence the test particle comes to a complete rest and does not move any more there. In other word, the test particle there satisfies the following conditions,

$$\begin{aligned} U_r &= U_\phi = 0 \\ \frac{dU_t}{d\tau} &= \frac{dU_r}{d\tau} = \frac{dU_\phi}{d\tau} = 0. \end{aligned}$$

For $U_r = U_\phi = 0$, the normalization condition $g^{\mu\nu}U_\mu U_\nu = -1$ yields $U_t = -(1 - 2M/r)^{1/2}$. Equations (20) and (22) satisfy the above conditions, and Plugging this $U_t = -(1 - 2M/r)^{1/2}$ together with $\frac{dU_r}{d\tau} = 0$ into equation (21) gives,

$$0 = -\left(\frac{M}{r^2}\right)\left(1-\frac{2M}{r}\right)^{-1/2} + \left(\frac{M}{r^2}\right)\left(1-\frac{2M}{r}\right)^{-1}\left(\frac{L^{\infty}}{L^{\infty}_{Edd}}\right). \tag{23}$$

The solution of Equation (23) gives the radial distance r_{so} of the "suspension orbit",

$$r_{so} = 2M\left[1-\left(\frac{L^{\infty}}{L^{\infty}_{Edd}}\right)^2\right]^{-1} \tag{24}$$

which is equivalent to the radial position of the critical point in Abramowicz et al.[5] and Bini et al.[8], and is determined by $\left(\frac{L^{\infty}}{L^{\infty}_{Edd}}\right)$ alone.

Since first term on the right-handed side in equation (23) denotes gravitational inward force exerted on the test particle at complete rest in the "suspension orbit" and second term refers to the outward radiation pressure there, equation (23) means that the gravitational inward force at the "suspension orbit" exactly balance the outward radiation pressure there.

It is interesting that among the entries/components of the radiation stress-energy tensor, the (t,t)-component, which is the radiation energy density and the (r,r)-component, which is the radiation pressure, exerts only on the moving particle, while the only (t,r)-component, which is the pressure gradient (force) exerts on both the stationary particle and the moving particle. As we already mentioned above, the (t,t) and (r,r) components of our choice of the stress-energy tensor are different from those of Bini et al.[8] whereas the (t,r) component of ours is exactly same as that of Bini et al.[8].

As a result, although the trajectory of the test particle before it reaches the "suspension orbit" in our study is manifestly different from that in the study of Bini et al.[8], once the test particle arrives at the "suspension orbit", the outward radiation pressure gradient that balance the inward gravitational force in our study is the same as that in the study of Bini et al.[8] and this is precisely why our radial distance of the "suspension orbit" and theirs turn out to be the same.

4 Concluding remarks

Although since the remarkable discovery first made by Poynting and Robertson, a number of study on this Poynting-Robertson effect have been performed, in almost all the works the luminous radiation source has been treated as being point-like. This could be due to their particular aims of investigations in which they just tried to eliminate unnecessary complexity which has little to do with essence of their studies. Largely, however, such simplification or reduction of the set-up can be attributed to the technical and computational difficulties. In

order to render the set-up for the careful and detailed investigation of the Poynting-Robertson effect to be more realistic and practical, obviously one has to take into account the finite size of the radiating source. Even in a very few works in the literature addressing this issue of finite size, the treatment of the issue has been very limited. For instance, Abramowicz et al. [5] attempted general relativistic and analytical approach, but they considered radial equation of motion alone. Next, Miller and Lamb [6,7] performed general relativistic and numerical approach, but they considered angular equation of motion alone. To summarize, even these few works addressing the issue of finite size effect for the Poynting-Robertson effect have remained essentially incomplete. Along this line, our present work can be regarded as comprehensive treatment of the finite size effects on the Poynting-Robertson effect in a fully general relativistic context for the first time ever. As a result of this comprehensive treatment of the problem, we were successful in realizing the existence of critical point/suspension orbit and in understanding the detailed characteristics of this suspension orbit. It is our hope, therefore, that the present study of ours could solve as a ground work on which further serious studies addressing the issue of finite size effects on the Poynting-Robertson effect can be successfully carried out.

Acknowledgments

J.S.O. acknowledges the support of the BK21 program to SNU.

References

[1] Poynting J. H., Phil. Trans. R. Soc. **203**, 525 (1903).

[2] Robertson H. P., M.N.R.A.S **97**, 423 (1937).

[3] Guess, A. W., Astrophys. J. **135**, 855 (1962).

[4] Carrol, D. L., Astrophys. J. **348**, 588 (1990).

[5] Marek A. Abramowicz, George F. R. Ellis, and Antonio Lanza, Astrophys. J. **361**, 470 (1990).

[6] M. Coleman Miller and Frederick K. Lamb, Astrophys. J. **413**, L43 (1993).

[7] M. Coleman Miller and Frederick K. Lamb, Astrophys. J. **470**, 1033 (1996).

[8] Donato Bini, Robert T Jantzen, and Luigi Stella, Class. Quantum Grav. **26**, 055009 (2009).

[9] Frederick K. Lamb and M. Coleman Miller, Astrophys. J. **439**, 828 (1995).

[10] J. M. Bardeen, Astrophys. J. **162**, 71 (1970).

[11] J. M. Bardeen, W. H. Press, and S. A. Teukolsky, Astrophys. J. **178**, 347 (1972).